Numerical approach of natural convection in eccentric annular spaces filled with hybrid nanofluids

B. Allouche[a], M. Djezzar[a*], T. Tayebi[a, b] and S. Allouche[a]

[a]*Energetic Physics Laboratory , Frères Mentouri Constantine 1 University, Constantine, Algeria*

[b]*Department of Mechanical Engineering, Faculty of Sciences and Technology, University of Bordj Bou Arrerid, Algeria*

*Corresponding author, email: mdjezzar@umc.edu.dz

Abstract

A numerical analysis of free convection in two horizontal eccentric cylinders filled with $aAl_2O_3\text{-}TiO_2$/water hybrid nanofluid is performed in this paper. The two internal and external cylindrical walls are maintained respectively at the temperature T_h and T_c with $T_h > T_c$. Theoretical correlations for the thermal conductivity and viscosity of the hybrid nanofluid were used in this study. The problem is treated by dimensionless governing equations which areformulated in bipolar coordinates and solved by the finite volume method. The effects of the Rayleigh number and the hybrid nanoparticles volume fraction on the natural convective heat transfer are examined. The results are shown as isotherms and streamline contours, as well as average and local Nusselt number profiles. It was found that the inclusion of the hybrid nanoparticles in the base fluid produced an increase in the heat transfer rate. In addition, increasing the volume fraction of the hybrid nanoparticles improves the heat transfer rate for all Rayleigh number values.

1. Introduction

Several engineering devices such as electronic cooling, solar energy, heat exchangers, thermal energy storage and nuclear power plants, which used conventional heat transfer fluids, obtain minimal performance on these systems in many industrial applications due to their low thermal conductivity [1]. For this reason, there have been several attempts since Maxwell [2] to improve these thermal performances by increasing thermal conductivity. Combining solid particles of a millimeter or a micrometer size and high thermal conductivity in base fluids such as water, ethylene glycol (EG), and motor oil can improve her thermal performance. The size of these solid particles poses problems for researchers because they lead to sedimentation and clogging on the flow passages and cause erosion on the passage walls, increasing the pressure drop on the installations. In 1995, Choi [3] offered an excellent alternative called nanofluid by preparing by dispersion of solid particles of nanometric size sash as Cu, CuO, Ag, Au, AgO, Al_2O_3, $TiO_2$and carbon nanotubes (CNT) in the classic base fluid. This new category makes it possible, on the one hand, to avoid problems due to sedimentation and clogging. On the other hand, they present significantly higher thermal properties so that the very high thermal conductivity of these solid nanoparticles compared to the base fluid can improve the heat transfer rate in various practical applications. Several well-developed studies were analyzed the heat transfer rate of nanofluids, such as those used in [4]–[11]. Recent Advances in Nanofluid Flow Modeling and Simulation (Fundamentals, Theory, and Applications) are summarized by Mahian et al. [12], [13].

Recently, researchers have been interested in enhancing or strengthening the thermal conductivity of nanoparticles by synthesizing hybrid nanoparticles to obtain a better improvement in heat transfer rate[14], [15].

Several research studies have investigated heat transfer and fluid flow using the hybrid nanofluid as a working fluid. We can mention: Kaskaet al. [16] conducted a CFD analysis to investigate the effect of AlN - Al_2O_3 hybrid nano powders on heat transfer and pressure inside a flat horizontal tube. They found that AlN - Al_2O_3 hybrid nanoparticles suspended in water as the base fluid significantly improve heat transfer. Hayat and Nadeem [17] Investigated a Three-dimensional stable rotating flow of hybrid nanofluid (Ag-CuO/water) with thermal radiation, heat generation and chemical reaction on a linearly stretched surface. It is concluded that even in the presence of radiation, heat generation and chemical reaction, the heat transfer rate of hybrid nanofluid is higher than that of single nanofluid. Yıldız et al. [18] conducted a comparative study to reveal the influence of theoretical and experimental correlations of thermal conductivity on the heat transfer performance of hybrid nanofluids. They showed that the use of theoretical models for thermal conductivity underestimates the heat transfer performance of mono and hybrid nanofluids. Ghaffarkhah et al. [19] experimentally investigated the dynamic viscosity of four different hybrid nano-lubricants containing COOH-functionalized MWCNTs and oxide nanoparticles. They used decision tree, random forest,

SVM and RBF-ANN to predict the viscosity of prepared nanofluids. They noticed that the dynamic viscosity of prepared hybrid nano-lubricants increases with increasing solid volume fraction and that the type of oxide nanoparticles has an insignificant effect on the dynamic viscosity of prepared hybrid nano-lubricants. SyamSundar et al. [20] prepared the hybrid nanofluids by dispersing synthesized GO/Co_3O_4 nanoparticles in water, ethylene glycol and ethylene glycol/water mixtures. Properties such as thermal conductivity and viscosity were estimated experimentally at different volume concentrations and temperatures. They found that the thermal conductivity enhancement of the water-based nanofluid is 19.14% and that of the ethylene glycol-based nanofluid is 11.85% compared to their respective base fluids. They also found that the improvement in viscosity of the water-based nanofluid is 1.70 times and that of the ethylene glycol-based nanofluid is 1.42 times. Sun et al. [21] experimentally analyzed the effects of adding different dispersants on the mixed nanofluids. They used silver (Ag)-multi-walled carbon nanotube/water hybrid nanofluids as a heat transfer medium. They found that heat transfer efficiency increases with increasing mass fraction. In addition, the results show that the thermal conductivity of hybrid Ag-multi-walled carbon nanotube/water nanofluids is higher than that of multi-walled carbon nanotube nanofluid. Baghbanzadeh et al. [22] studied the effects of silica nanospheres, multi-walled carbon nanotubes (MWCNTs) and two types of their hybrids on the viscosity and density of distilled water. They found that the viscosity and density of nanofluids increased with concentration, while they decreased with increasing temperature.

The published articles are generally dealing with specific annular spaces which are available in various configurations like circular, rectangular, elliptical, triangular and square, as well as in concentric and eccentric configurations. Research on nanofluid flow and heat transfer in a concentric and eccentric circular annular passage has been reported: Gholamalipour et al. [23] investigated a numerical study on the heat transfer by free convection and the generation of entropy of the Cu-water nanofluid inside an annulus, filled with a porous foam, in the presence of a cylindrical heat source. They applied the two-phase mixture model and used Corcione's correlations to calculate the viscosity and thermal conductivity of the mixture. They examined the effects of the vertical and horizontal eccentricity of the heat source and the volume fraction of the nanoparticles for different values of Darcy and Rayleigh numbers on heat transfer and entropy generation. They found that for various eccentricity figures, the heat transfer can be improved or deteriorated, depending on the value of Da, Ra and the eccentricity. Therefore, for each Rayleigh number, optimal values of Da and e exist to achieve the maximum average Nu number. Moreover, the eccentric annulus down expresses the best performance in which the highest heat transfer and the lowest entropy generation occur. Hu et al. [24]

investigated natural convection numerically in an eccentric annulus filled with Cu-water nanofluid with a constant heat flux wall. They treated the boundary conditions of Dirichlet and Neumann using the immersed boundary method (IBM). The governing equations of the flow and temperature fields are solved by the lattice Boltzmann method (LBM). They investigated the Influences of Rayleigh number, eccentricity, nanoparticle volume fraction and radial ratio on the streamlines, isotherms and the Nusselt number. They found that the inclusion of the nanoparticles into pure fluid changes the flow pattern. Moreover, the Nusselt number has a positive relationship with nanoparticle volume fraction, the Rayleigh number and the radial ratio. Tayebi et al. [25] did a numerical study to explain the impact of the presence of a solid conductive partition on the heatless convective motion mechanism and heat transmission process in a concentric circular annulus filled with a hybrid nanoliquid at water-based containing copper and alumina nanoparticles. They interpreted the influence of selected factors such as nanoparticle concentration, Rayleigh number, fluid/solid thermal conductivity ratio and IHG/A parameter on thermo-hydrodynamic behavior and heat exchange rate. They showed that in the presence of a solid conductive wall, the combined effects of the IHG/A phenomenon and of the combined nanoparticles considerably modify the behavior of flow and heat exchange within the annulus. Tayebi and Chamkha [26] used the finite volume method to numerically analyze natural convection in an eccentric space between two horizontal cylinders filled with hybrid $Cu–Al_2O_3$/water nanofluids. They performed a numerical parametric study for an annular space filled with ordinary water, Al_2O_3/water nanofluid and hybrid $Cu–Al_2O_3$/water nanofluid for various volume fractions of nanoparticles and hybrid nanoparticles ($0 \le \varphi \le 0.12$) and Rayleigh ($10^3 \le Ra \le 10^6$). The inner wall of the cylinder is heated to a uniform temperature while the outer wall is kept isothermal cooled. They found that using a hybrid $Cu–Al_2O_3$/water nanofluid gives better thermal and dynamic enhancement than a similar Al_2O_3/water nanofluid.

According to the best authors' knowledge, this is the first attempt to use the extended model of Maxwell to investigate the natural convective flow of Al_2O_3-TiO_2/water hybrid nanofluid inside an eccentric annulus with an angular position θ=0°. Therefore, the purpose of this study is to numerically analyze natural convection in an eccentric annulus filled with an Al_2O_3-TiO_2/water hybrid nanofluid. The inner and outer walls of the annular space are brought to different constant and uniform temperatures. An extended model of Maxwell [27] was used for the calculation of the thermal conductivity of the hybrid nanofluid. To carry out the calculations we have fixed the annulus radius ratio and the eccentricity to 2.4 and 0.6, respectively and the azimuthal angle to 90° and 0°. The effects of the Rayleigh number ($10^3 \le Ra \le 10^6$) and the hybrid nanofluid volume fraction ($0 \le \varphi \le 0.04$) on the heat transfer by natural convection are examined in this study.

2. Mathematical Formulation

2.1. Description of the Problem

The physical domain is shown in Figure. 1. Consider an annular space between two horizontal eccentric cylinders filled with water-based hybrid nanofluid which is incompressible Newtonian fluid. The two internal and external cylinders are maintained respectively at the temperatures T_h and T_c with $T_h>T_c$. The eccentricity is defined by E, where E is the distance between the centers of the two cylinders. $D_h=r_o-r_i$, is the hydraulic diameter where r_i and r_o are the inner and outer radii of the cylinder, respectively.

Under the single-phase nanofluid model, the liquid phase and the solid nanoparticles are in thermal equilibrium. The flow is two-dimensional, permanent and laminar. The heat transfer by radiation and the viscous dissipation are negligible. With the exception of the density, which adopts the Boussinesq approximation in terms of Archimedes' force, the thermophysical properties are considered constant.
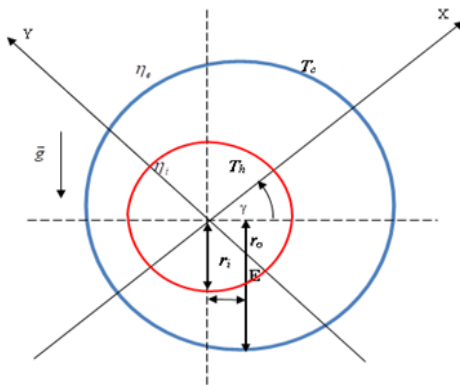
Figure 1. The geometric configuration

Table1: The thermophysical properties of the nanoparticles and the base fluid

thermophysical properties	Al$_2$O$_3$	TiO$_2$	water
ρ(Kg.m^3)	3970	4250	997.1
Cp(J. Kg^{-1}. K^{-1})	765	686.2	4179
λ(W.m^{-1}. K^{-1})	40	8.954	0.613
β(K^{-1}).10^{-5}	0.85	0.9	21

The thermophysical properties of water and nanoparticles are listed in Table 1. The Al$_2$O$_3$–TiO$_2$/waterhybrid nanofluid is used in the present study. The effective thermal conductivity and viscosity of the present hybrid nanofluid can be calculated by Maxwell's extended model [27] and Brinkman's model [28] as:

$$\lambda_{hnf} = \lambda_f \left[1 + \frac{3\left(\frac{\lambda_{Al_2O_3}}{\lambda_f}-1\right)0.75\varphi}{\left(\frac{\lambda_{Al_2O_3}}{\lambda_f}+2\right)-\left(\frac{\lambda_{Al_2O_3}}{\lambda_f}-1\right)0.75\varphi} + \frac{3\left(\frac{\lambda_{TiO_2}}{\lambda_f}-1\right)0.25\varphi}{\left(\frac{\lambda_{TiO_2}}{\lambda_f}+2\right)-\left(\frac{\lambda_{TiO_2}}{\lambda_f}-1\right)0.25\varphi} \right] \quad (1)$$

$$(\mu)_{hnf} = \frac{\mu_f}{(1-\varphi)^{2.5}} \quad (2)$$

With: $\quad \varphi = \varphi_{Al_2O_3} + \varphi_{TiO_2} \quad (3)$

$\varphi_{Al_2O_3}$ and φ_{TiO_2} denote the volume fraction of two nanoparticles dispersed in water. Therefore, the total particle volume fraction is the sum of two concentrations of nanoparticles.

Also,φ and the subscripts f, hp and hnf denote respectively the volume fraction of the hybrid nanoparticles, the fluid phase, hybrid nanoparticle and the hybrid nanofluid. Based on the mixing law, the density, heat capacity, and thermal expansion of the hybrid nanofluid are determined as follows:

$$(\rho)_{hnf} = \varphi(\rho)_{hp} + (1-\varphi)\rho_f \quad (4)$$

$$(\rho)_{hp} = \frac{\varphi_{Ag}\rho_{Ag} + \varphi_{MgO}\rho_{MgO}}{\varphi} \quad (5)$$

$$(\rho Cp)_{hnf} = \varphi(\rho Cp)_{hp} + (1-\varphi)(\rho Cp)_f \quad (6)$$

$$(\rho Cp)_{hp} = \frac{\varphi_{Al_2O_3}(\rho Cp)_{Al_2O_3} + \varphi_{TiO_2}(\rho Cp)_{TiO_2}}{\varphi} \quad (7)$$

$$(\rho\beta)_{hnf} = \varphi(\rho\beta)_{hp} + (1-\varphi)(\rho\beta)_f \quad (8)$$

$$(\rho\beta)_{hp} = \frac{\varphi_{Al_2O_3}(\rho\beta)_{Al_2O_3} + \varphi_{TiO_2}(\rho\beta)_{TiO_2}}{\varphi} \quad (9)$$

2.2. Dimensional equations

To convert from Cartesian to bipolar coordinates, we employ the following relations:

$$x = a\frac{sh(\eta)}{ch(\eta)-\cos(\theta)} \quad y = a\frac{\sin(\theta)}{ch(\eta)-\cos(\theta)} \quad (10)$$

The dimensional continuity, energy and momentum equations given in bipolar coordinates are as follows:

$$\frac{\partial}{\partial\eta}(hV_\eta) + \frac{\partial}{\partial\theta}(hV_\theta) = 0 \quad (11)$$

$$V_\eta\frac{\partial T}{\partial\eta} + V_\theta\frac{\partial T}{\partial\theta} = \frac{\lambda_{hnf}}{(\rho C_P)_{hnf}}\frac{1}{h}\left[\frac{\partial^2 T}{\partial\eta^2} + \frac{\partial^2 T}{\partial\theta^2}\right] \quad (12)$$

$$V_\eta \frac{\partial \omega}{\partial \eta} + V_\theta \frac{\partial \omega}{\partial \theta} = g \frac{(\rho\beta_T)_{hnf}}{\rho_{hnf}} \left\{ \begin{array}{l} [F(\eta,\theta)\cos(\alpha)+G(\eta,\theta)\sin(\alpha)]\frac{\partial T}{\partial \eta} \\ +[F(\eta,\theta)\sin(\alpha)-G(\eta,\theta)\cos(\alpha)]\frac{\partial T}{\partial \theta} \end{array} \right\} \\ + \frac{1}{h}\frac{\mu_{hnf}}{\rho_{hnf}}\left[\frac{\partial^2 \omega}{\partial \eta^2}+\frac{\partial^2 \omega}{\partial \theta^2}\right] \qquad (13)$$

With:

$$h = a\left[ch(\eta)-\cos(\theta)\right]^{\frac{1}{2}}$$
$$F(\eta,\theta) = \frac{1-ch(\eta)\cos(\theta)}{ch(\eta)-\cos(\theta)} \qquad (14)$$
$$G(\eta,\theta) = \frac{\sin(\theta)sh(\eta)}{ch(\eta)-\cos(\theta)}$$

2.3. Dimensionless equations

The following quantities are used in order to convert dimensional equations into dimensionless equations:

$$D_h = r_o - r_i, \quad H = \frac{h}{D_h}, \quad V_\eta^+ = V_\eta \frac{D_h}{\alpha_f}, \quad V_\theta^+ = V_\theta \frac{D_h}{\alpha_f}, \quad \psi^+ = \frac{\psi}{\alpha_f},$$

$$\omega^+ = \omega \frac{D_h^2}{\alpha_f}, \quad T^+ = \frac{T-T_F}{T_C-T_F} \qquad (15)$$

The non-dimensionalized equations are:

$$\frac{\partial}{\partial \eta}\left(HV_\eta^+\right)+\frac{\partial}{\partial \theta}\left(HV_\theta^+\right)=0 \qquad (16)$$

$$HV_\eta^+ \frac{\partial T^+}{\partial \eta} + HV_\theta^+ \frac{\partial T^+}{\partial \theta} = \frac{\lambda_{hp}/\lambda_f}{\left[(1-\phi)+\phi\frac{(\rho C_P)_{hp}}{(\rho C_P)_f}\right]}\left[\frac{\partial^2 T^+}{\partial \eta^2}+\frac{\partial^2 T^+}{\partial \theta^2}\right] \qquad (17)$$

$$HV_\eta^+ \frac{\partial \omega^+}{\partial \eta} + HV_\theta^+ \frac{\partial \omega^+}{\partial \theta} = Ra_T \Pr H\left(\frac{1}{1+\frac{(1-\varphi)\rho_f}{\varphi\rho_{hp}}}\frac{\beta_{hp}}{\beta_f}+\frac{1}{1+\frac{\varphi\rho_f}{(1-\varphi)\rho_{hp}}}\right) \qquad (18)$$

$$\left\{ \begin{array}{l} [F(\eta,\theta)\cos(\alpha)+G(\eta,\theta)\sin(\alpha)]\frac{\partial T^+}{\partial \eta} \\ +[F(\eta,\theta)\sin(\alpha)-G(\eta,\theta)\cos(\alpha)]\frac{\partial T^+}{\partial \theta} \end{array} \right\} + \frac{(\mu)_{hnf}}{(\mu)_f}\frac{\Pr}{\left[\varphi\frac{\rho_{hp}}{\rho_f}+(1-\varphi)\right]}\left[\frac{\partial^2 \omega^+}{\partial \eta^2}+\frac{\partial^2 \omega^+}{\partial \theta^2}\right]$$

Where the components of the dimensionless velocity, and vorticity, are defined by:

$$V_\eta^+ = \frac{1}{H}\frac{\partial \psi^+}{\partial \theta},$$
$$V_\theta^+ = -\frac{1}{H}\frac{\partial \psi^+}{\partial \eta}, \qquad (19)$$
$$\omega^+ = -\frac{1}{H^2}\left[\frac{\partial^2 \psi^+}{\partial \eta^2}+\frac{\partial^2 \psi^+}{\partial \theta^2}\right]$$

The above equations are related to the following boundary conditions:

Inner cylinder surface conditions ($\eta = \eta_i$ constant):

$$T_1^+ = 1 \qquad (20)$$

$$V_\eta^+ = V_\theta^+ = \frac{\partial \psi^+}{\partial \theta} = \frac{\partial \psi^+}{\partial \eta} = 0 \qquad (21)$$

$$\omega^+ = -\frac{1}{H^2}\left[\frac{\partial \psi^+}{\partial \eta}+\frac{\partial \psi^+}{\partial \theta}\right]=0 \qquad (22)$$

Outer cylinder surface conditions ($\eta = \eta_e$ constant):

$$T_2^+ = 0 \qquad (23)$$

$$V_\eta^+ = V_\theta^+ = \frac{\partial \psi^+}{\partial \theta} = \frac{\partial \psi^+}{\partial \eta} = 0 \qquad (24)$$

$$\omega^+ = -\frac{1}{H^2}\left[\frac{\partial \psi^+}{\partial \eta}+\frac{\partial \psi^+}{\partial \theta}\right]=0 \qquad (25)$$

The following relationships, respectively, describe the Prandtl number, Rayleigh number, and local and average Nusselt numbers on the inner cylinder wall:

$$\Pr = \frac{\upsilon}{\alpha_T} \qquad (26)$$

$$Ra_T = \frac{g\beta_T D_h^3}{\alpha_f \upsilon}\Delta T \qquad (27)$$

$$Nu_{local} = -\frac{\lambda_{hnf}}{\lambda_f}\frac{1}{H}\frac{\partial T^+}{\partial \eta}\bigg|_{\eta=cst} \qquad (28)$$

$$Nu = \frac{1}{\theta_{NN}-\theta_1}\int_{\theta_1}^{\theta_{NN}} Nu_{local}.d\theta \qquad (29)$$

3. Solution procedure and validation

Finite volume method is chosen to discretize the partial differential equations of the parabolic type. On the other hand, we have chosen the Taylor series development to discretize the partial differential equation of the elliptic type. An iterative method (the Gauss-Seidel method) with a sub-relaxation process is used to solve the resultant system of algebraic equations. The following criterion is used to achieve convergence:

$$\left|\frac{\max \varphi^{n+1}-\max \varphi^n}{\max \varphi^{n+1}}\right| \leq 10^{-6}$$

3.1. Mesh Study

Table 2 presents the mesh test procedure to examine the independence of the grid on the numerical results by calculating the maximum stream function values and the average Nusselt number around the inner cylinder wall. The choice of mesh influences the accuracy of the results. Several meshes are used for the following configuration: $Ra = 10^4$, $\varphi = 0.04$, $r = 2.4$, $e = 0.6$ and $\theta=90°$. The table shows the variation of the average Nusselt number and the maximum stream function values according to the number of nodes and allows us to choose the mesh 51×101. We opt for the mesh (51×101) to have a good compromise between precision and computation time.

Table 2: Relations used for the thermo-physical properties of hybrid nanofluids

Grid size	11×21	21×41	31×61	41×81	51×101	61×121
Nu $_{avg}$	3.796	3.916	3.996	4.075	4.159	4.246
Er (%)	-	3.06	2.00	1.93	2.01	2.04
Ψ $_{Max}$	26.11	22.86	21.87	21.41	21.13	20.94

3.2. Code Validation

A comparison of the dimensionless temperature profile between two concentric cylinders of the present study with the numerical results obtained by Cho et al. [29] and L.S. Yao et al. [30]for r=2.6, Pr=0.706, e=0.652, φ=0, θ=90° and Ra=4.8×10^4 is represented in figure 2. The results of the present study agree well with those of references [29] and [30].
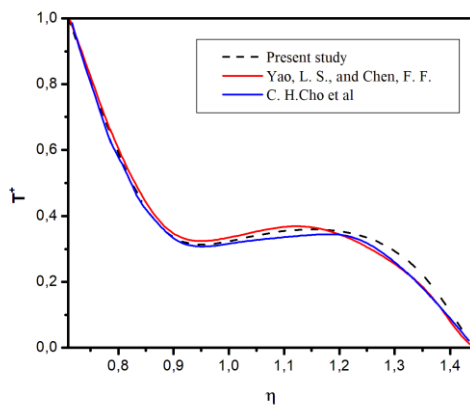
Figure 2. Comparison of the dimensionless temperature profile with two references [29]and [30]for the concentric annulus.

4. Results and discussion

The present study considers a horizontal eccentric annular space filled with Al_2O_3-TiO_2/water hybrid nanofluid. The effect of hybrid nanofluids on natural convection flow and heat transfer is examined. The thermophysical properties of the nanoparticles and of the basic fluid are given in Table 1. The calculations are carried out for different values of Rayleigh number and volume fraction of nanoparticles. We have fixed the radius ratio and the eccentricity to 2.4 and 0.6, respectively and the azimuthal angle to 90° and 0°. The results are presented in the form of streamlines, isotherms, local and average Nusselt number.

The figure 3 illustrates the distribution of isotherms and streamlines for a Rayleigh number Ra=10^4 when θ=90° and φ=0.04. It is shown that the flow and the thermal field are symmetrical with respect to thecylinder's vertical axis. In this case, when the inner wall of the cylinder heats up, the temperature of the hybrid nanofluid near the wall rises and the hot hybrid nanofluid moves upwards while the cold hybrid nanofluid moves downwards. Therefore, the flow is organized into two cells which rotate in the clockwise direction on the left side, and in the counterclockwise direction on the right side. The temperature distribution decreases as one approaches the cold wall. The isotherms deform and adopt the shape of a mushroom,

Isotherms and streamlines contours for different values of Rayleigh number when θ=0° and φ=0.04 are shown in Figure 4. We observe that the symmetry has disappeared when θ=0°. The isotherms lean towards the right region of the annular space and are essentially organized on the enlarged right side. This is due to the inhibition of flow between the inner and outer left walls of the annular space. In addition,it was indicated that the flow and the thermal fields were notably affected by the variation of the Rayleigh number. When the Rayleigh number is relatively small, Ra=10^3, the maximum value of the stream function, as shown in the figure, is small and the isotherms are slightly deformed on the upper right part of the heated wall, implying that the heat transfer by conduction between the outer and inner cylinders is dominated. When Ra=10^4, the isothermal lines change significantly, as does the maximum value of the stream function, indicating a transformation from conductive to convective heat transfer regime. For Ra=10^5, the convection intensifies, so the flow becomes very intense and the maximum value of the stream function increases. The isotherm contours become extremely distorted and adopt the shape of a mushroom.

Figure 5 presents the isotherms and streamlines for the Rayleigh number Ra=10^5 and different volume fraction values when θ=0°. The figures show that the flow and the thermal fields depend on the volume fraction variation. It is observed that the isotherms deform slightly with the increase in the volume fraction and it is noted that the maximum value of the stream function indicated in the figure increases with the increase in the volume fraction of

hybrid nanofluid, which implies an intensification of natural convection. Moreover, the different values of the stream function show that that the enhancement of the heat transfer rate of the hybrid nanofluid is more pronounced compared to the base fluid.
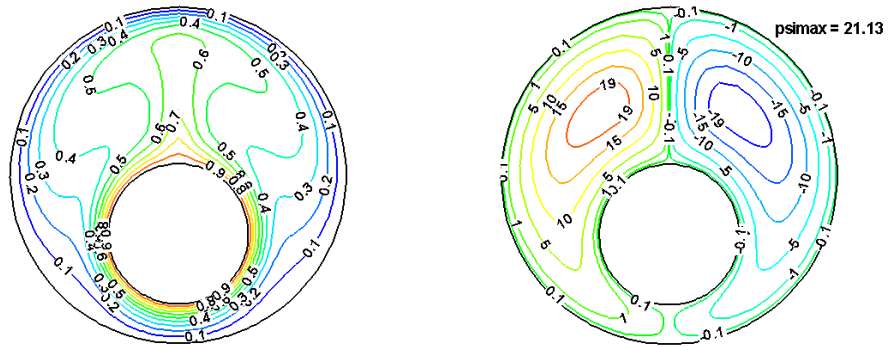
Figure 3. Streamlines and Isotherms for a volume fraction φ=0.04, θ=90° and Ra=10⁴

Ra = 10^3

Ra = 10^4

Ra = 10⁵
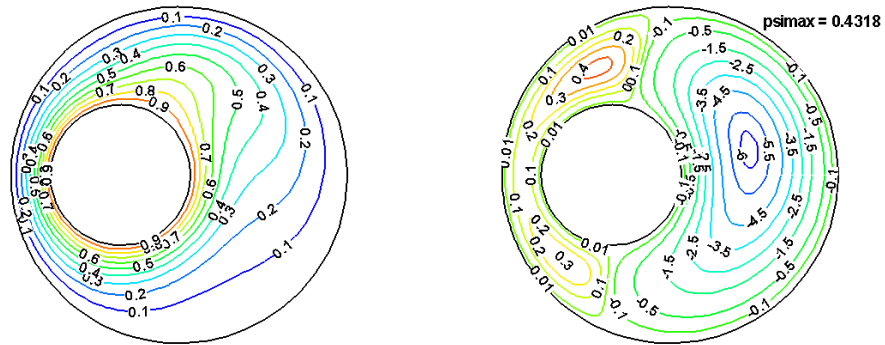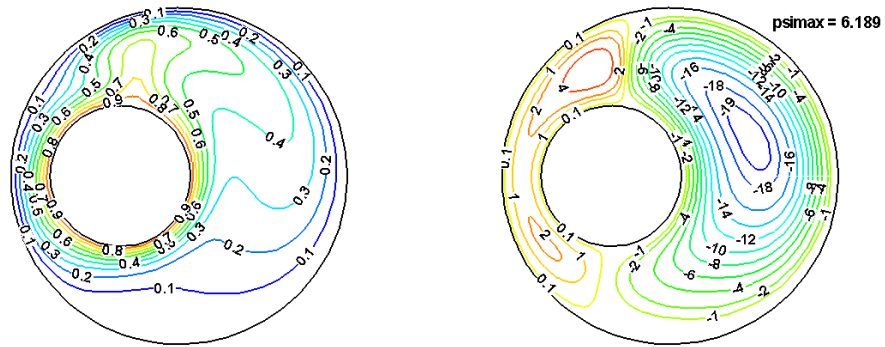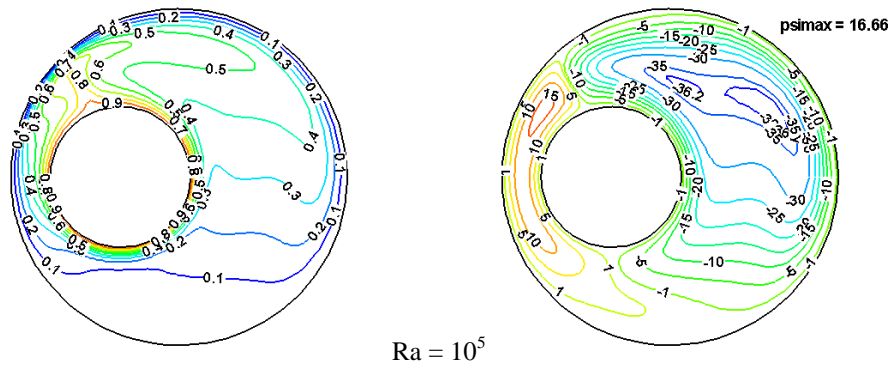
Figure 4. Streamlines and Isotherms for different Rayleigh numbers

φ = 0 %

φ = 1 %

φ = 2 %

φ = 3 %

φ = 4 %
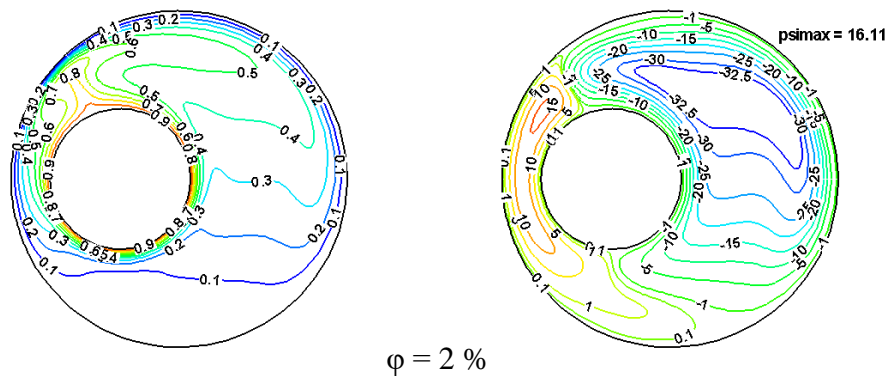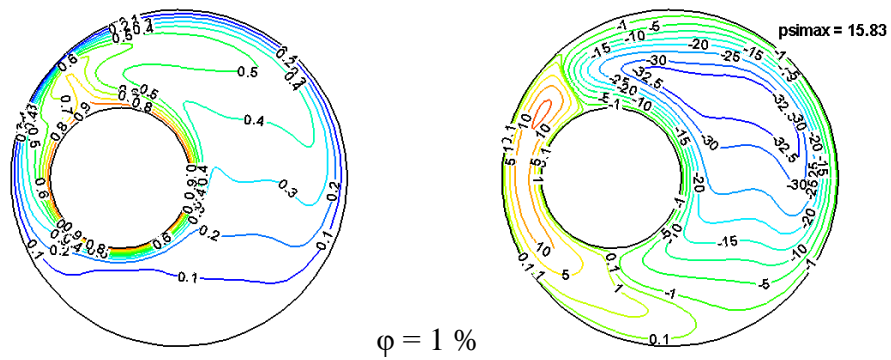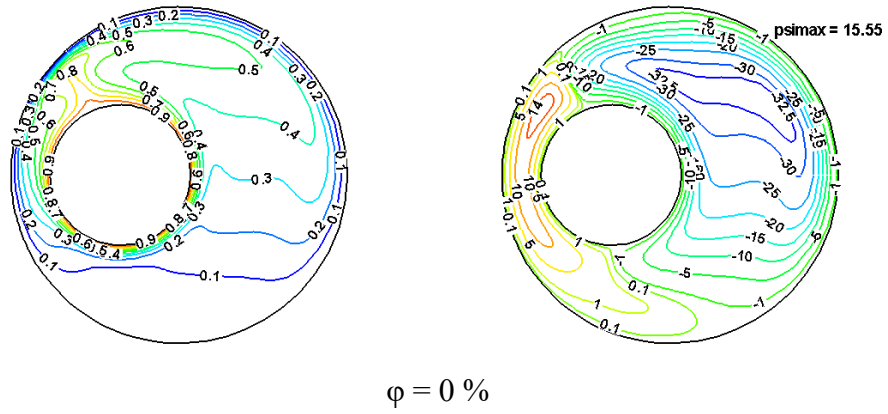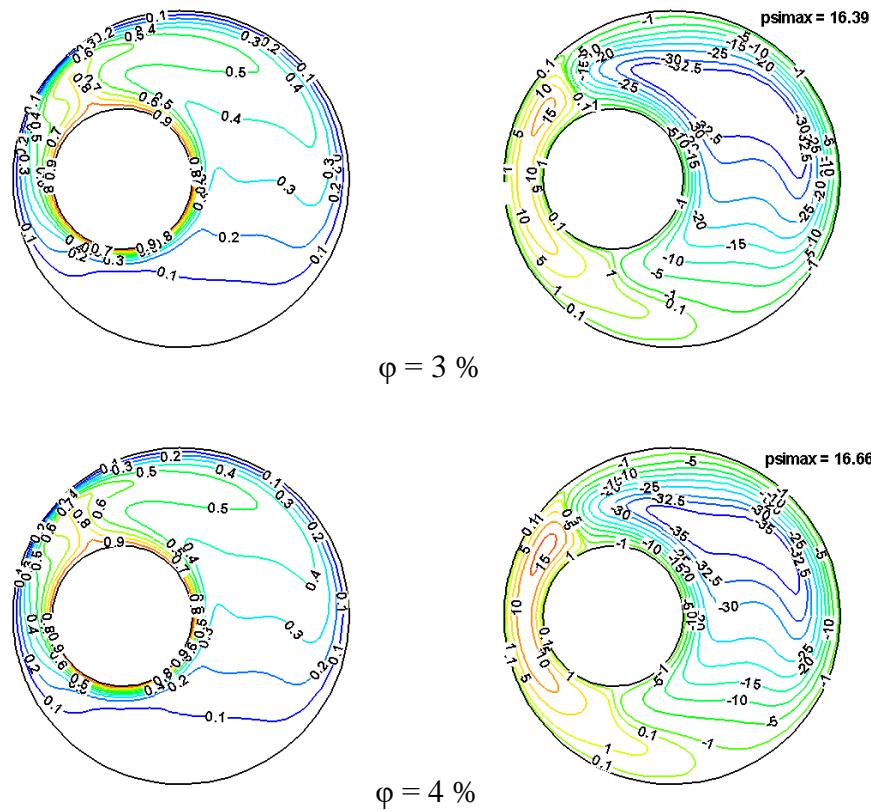
Figure 5. Streamlines and Isotherms for different volume fractions

The comparison between variations of local Nusselt numbers along the inner wall for different values of the volume fraction when Ra $=10^3$, 10^4 and 10^5 is shown in Figure 6. The figure shows that increasing the Rayleigh number increases the value of the local Nusselt number. The curves show that for a Rayleigh number Ra$=10^3$ where conduction dominates and the isotherms are nearly parallel circles, the local Nusselt number begins to decrease until it reaches a minimum number at θ=45° then it increases and reaches its maximum value at the azimuthal position θ=180°. For Ra$=10^4$ and Ra$=10^5$, the heat transfer dominates by the convection mode between the two walls of the space. In this case, the local Nusselt number is minimum at θ=60° for Ra$=10^4$ and θ=90° for Ra$=10^5$ and maximum at the azimuthal position θ=315° for Ra$=10^4$ and Ra$=10^5$. It is noticed that when the volume

fraction increases the variation of the local Nusselt number along the wall increases for the Rayleigh values 10^3,10^4 and 10^5, which means that the increase in the volume fraction improves the heat transfer rate for the considered values of the Rayleigh number.

Figure 7 depicts the effects of the hybrid nanofluid volume fraction on the mean Nusselt number for each Rayleigh number considered. Figures show that the average Nusselt number increases significantly with increasing Rayleigh number and slightly with increasing volume fraction. Each figure shows that increasing the volume fraction of the hybrid nanofluids for the given Rayleigh number raises the average Nusselt number, implying an improvement in heat transfer rate as a function of volume fraction.
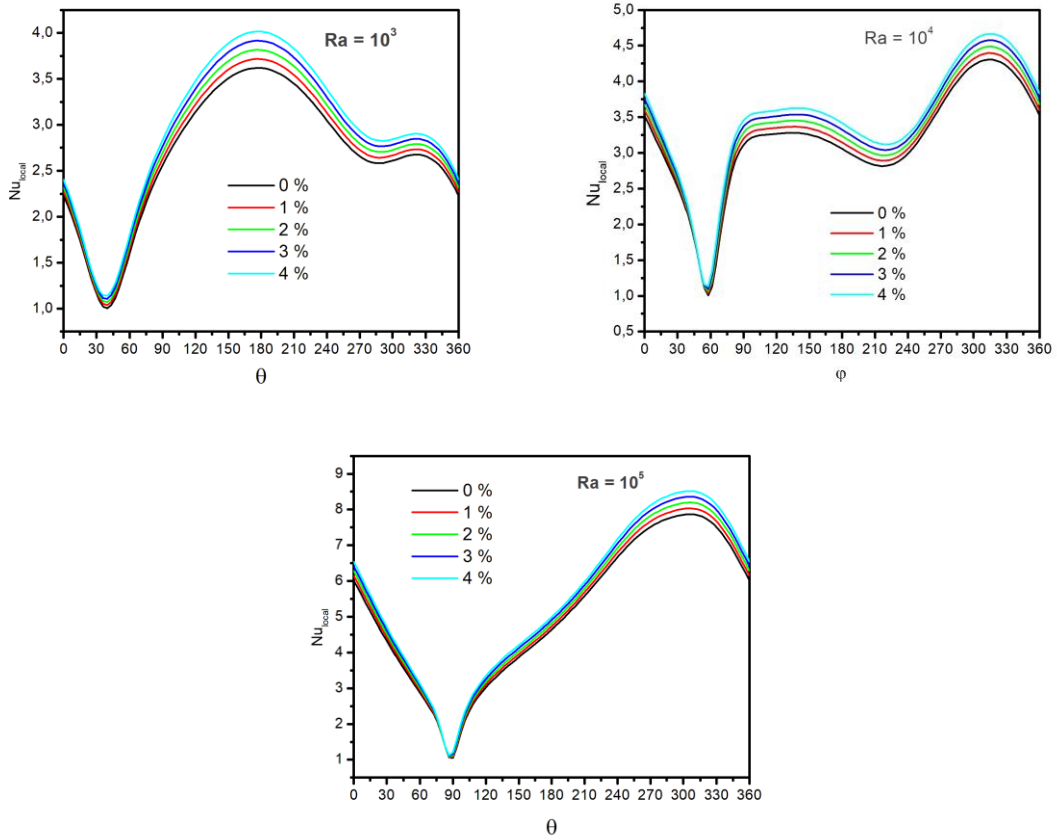
Figure 6. Comparison of variations of local Nusselt numbers on the inner wall for different volume fractions
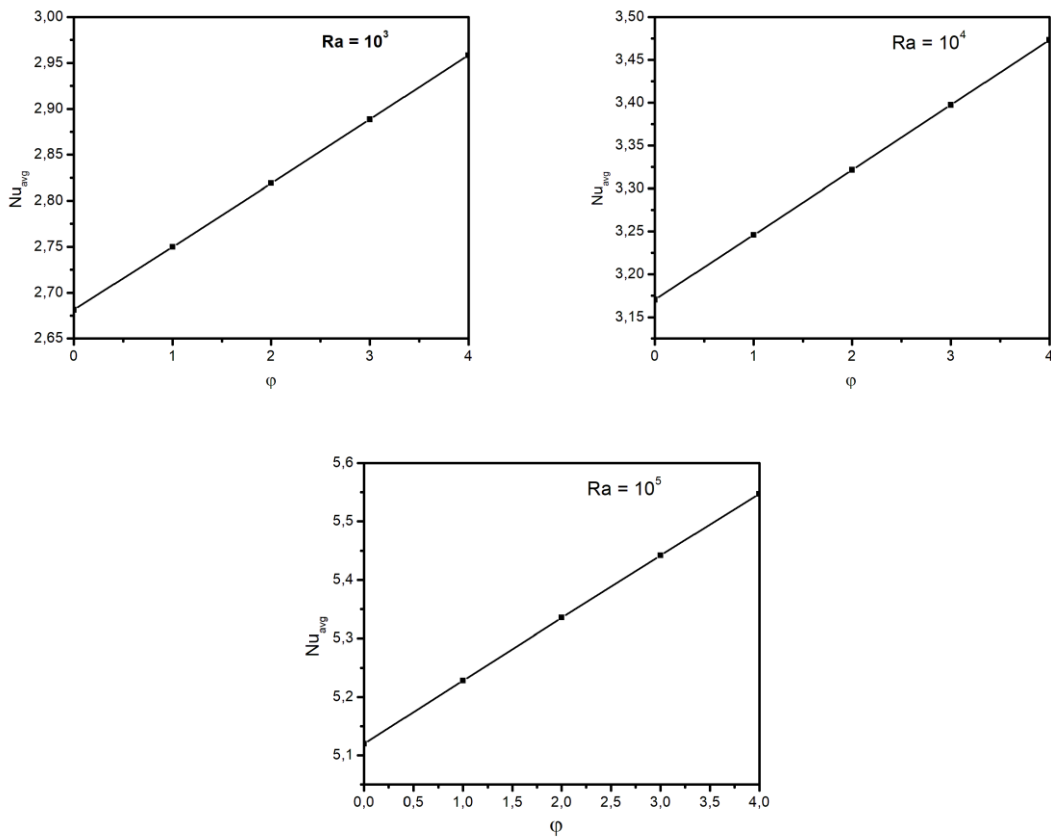
Figure 7. Variation of the average Nusselt number as a function of the volume fraction

51

5. Conclusion

In this paper, natural convection flow and heat transfer in an eccentric annular space filled with a hybrid nanofluid was analyzed numerically. The finite volume method was used to numerically solve the system of governing equations with the boundary conditions. The obtained results are highlighted for the following parameters: the ratio of the annular radius r=2.4, the eccentricity e=0.6 and the azimuth angle at 90° and 0° by considering the effect of the Rayleigh number ($10^3 \leq Ra \leq 10^5$) and the volume fraction of nanoparticles ($0 \leq \varphi \leq 4\%$) on the flow behavior and heat transfer rate. The results obtained can be summarized in the following points:

- The heat transfer enhancement could be obtained for high values of Rayleigh number.
- The heat transfer is better in the hybrid nanofluid compared to the base fluid.
- For all values of the Rayleigh number, local and average Nusselt numbers increase with the increase of the volume fraction of nanoparticles, so adding the hybrid nanoparticles to the base fluid improves the heat transfer rate in an eccentric annular space.

Nomenclature

Cp specific heat (J. kg^{-1}. K^{-1})

D_h hydraulic diameter (m)

E distance between the centers of the two cylinders (m)

e dimensionless eccentricity E ÷ (r_o - r_i)

g gravitational acceleration (m. s^{-2})

h scale factor (m)

H dimensionless scale factor

Nu Nusselt number

Pr Prandtl number

r radius ratio

Ra Rayleigh number

r_i inner and outer radii of annulus (m)

r_o inner and outer radii of annulus (m)

T dimensional temperature (K)

T$^+$ dimensionless temperature (K)

V_η velocity components in the η direction (m.s^{-1})

V_η^+ dimensionless velocity components in the η direction

V_θ velocity components in the θ direction (m.s^{-1})

V_θ^+ dimensionless velocity components in the θ direction

x, y Cartesian coordinates (m)

Greek symbols

α thermal diffusivity (m^2. s^{-1})

β thermal expansion coefficient (K^{-1})

γ orientation angle of the annulus (°)

η first bipolar coordinate

θ second bipolar coordinate

λ thermal conductivity (W.m^{-1}. K^{-1})

μ dynamic viscosity (kg.m^{-1}. s^{-1})

ρ density (kg.m^{-3})

υ kinematic viscosity (m^2.s^{-1})

ψ stream function (m^2. s^{-1})

ω vorticity (s^{-1})

Subscripts

c cold

f fluid

h hot

hnf hybrid nanofluid

hp hybrid solid particles

i inner cylinder

o outer cylinder

References

[1] M. Akbari, N. Galanis, and A. Behzadmehr, Comparative analysis of single and two-phase models for CFD studies of nanofluid heat transfer, International Journal of Thermal Sciences. 50 (2011) 1343-1354.

[2] J. C. Maxwell, treatise on electricity and magnetism.(Ed.), 1873.

[3] S. U. S. Choi and J. A. Eastman, enhancing thermal conductivity of fluids with nanoparticles. (1995).

[4] E. Abu-Nada and A. J. Chamkha, Effect of nanofluid variable properties on natural convection in enclosures filled with a CuO-EG-Water nanofluid, International Journal of Thermal Sciences. 49 (2010) 2339-2352.

[5] H. K. Dawood, H. A. Mohammed, and K. M. Munisamy, Heat transfer augmentation using nanofluids in an elliptic annulus with constant heat flux boundary condition, Case Studies in Thermal Engineering. 4 (2014) 32-41.

[6] A. Doostani, M. Ghalambaz, and A. J. Chamkha, MHD natural convection phase-change heat transfer in a cavity: analysis of the magnetic field effect, J Braz. Soc. Mech. Sci. Eng. 39 (2017) 2831-2846.

[7]   H. F. Öztop, A. Sakhrieh, E. Abu-Nada, and K. Al-Salem, Mixed convection of MHD flow in nanofluid filled and partially heated wavy walled lid-driven enclosure,International Communications in Heat and Mass Transfer. 86 (2017) 42–51.

[8]   M. Habibi Matin and I. Pop, Natural convection flow and heat transfer in an eccentric annulus filled by Copper nanofluid, International Journal of Heat and Mass Transfer. 61 (2013) 353–364.

[9]   E. Abu-Nada, Z. Masoud, and A. Hijazi, Natural convection heat transfer enhancement in horizontal concentric annuli using nanofluids, International Communications in Heat and Mass Transfer. 35 (2008) 657–665.

[10] A. Bouzerzour, M. Djezzar, H. F. Oztop, T. Tayebi, and N. Abu-Hamdeh, Natural convection in nanofluid filled and partially heated annulus: Effect of different arrangements of heaters, Physica A: Statistical Mechanics and its Applications. 538 (2020) 122479.

[11] A. Bouzerzour, T. Tayebi, A. J. Chamkha, and M. Djezzar, Numerical investigation of natural convection nanofluid flow in an annular space between confocal elliptic cylinders at various geometrical orientations Comput Thermal Scien. 12 (2020) 99–114.

[12] O. Mahian et al., Recent advances in modeling and simulation of nanofluid flows-Part I: Fundamentals and theory, Physics Reports. 790 (2019) 1–48.

[13] O. Mahian et al., Recent advances in modeling and simulation of nanofluid flows—Part II: Applications, Physics Reports. 791 (2019) 1–59.

[14] T. Tayebi and A. J. Chamkha, Buoyancy-driven heat transfer enhancement in a sinusoidally heated enclosure utilizing hybrid nanofluid, Comput Thermal Scien. 9 (2017) 405–421.

[15] S. Suresh, K. P. Venkitaraj, P. Selvakumar, and M. Chandrasekar, Synthesis of Al_2O_3–Cu/water hybrid nanofluids using two step method and its thermo physical properties, Colloids and Surfaces A: Physicochemical and Engineering Aspects. 388 (2011) 41–48.

[16] S. A. Kaska, R. A. Khalefa, and A. M. Hussein, Hybrid nanofluid to enhance heat transfer under turbulent flow in a flat tube, Case Studies in Thermal Engineering. 13 (2019) 100398.

[17] T. Hayat and S. Nadeem, Heat transfer enhancement with Ag–CuO/water hybrid nanofluid, Results in Physics. 7 (2017) 2317–2324.

[18] Ç. Yıldız, M. Arıcı, and H. Karabay, Comparison of a theoretical and experimental thermal conductivity model on the heat transfer performance of Al_2O_3-SiO_2/water hybrid-nanofluid, International Journal of Heat and Mass Transfer. 140 (2019) 598–605.

[19] A. Ghaffarkhah, A. Bazzi, Z. Azimi Dijvejin, M. Talebkeikhah, M. Keshavarz Moraveji, and F. Agin, Experimental and numerical analysis of rheological characterization of hybrid nano-lubricants containing COOH-Functionalized MWCNTs and oxide nanoparticles, International Communications in Heat and Mass Transfer. 101 (2019) 103–115.

[20] L. Syam Sundar, M. K. Singh, M. C. Ferro, and A. C. M. Sousa, Experimental investigation of the thermal transport properties of graphene oxide/Co 3 O 4 hybrid nanofluids, International Communications in Heat and Mass Transfer. 84 (2017) 1–10.

[21] B. Sun, Y. Zhang, D. Yang, and H. Li, Experimental study on heat transfer characteristics of hybrid nanofluid impinging jets, Applied Thermal Engineering. 151 (2019) 556–566.

[22] M. Baghbanzadeh, A. Rashidi, A. H. Soleimanisalim, and D. Rashtchian, Investigating the rheological properties of nanofluids of water/hybrid nanostructure of spherical silica/MWCNT, Thermochimica Acta. 578 (2014) 53–58.

[23] P. Gholamalipour, M. Siavashi, and M. H. Doranehgard, Eccentricity effects of heat source inside a porous annulus on the natural convection heat transfer and entropy generation of Cu-water nanofluid, International Communications in Heat and Mass Transfer. 109 (2019) 104367.

[24] Y. Hu, D. Li, S. Shu, and X. Niu, Natural convection in a nanofluid-filled eccentric annulus with constant heat flux wall: A lattice Boltzmann study with immersed boundary method, International Communications in Heat and Mass Transfer. 86 (2017) 262–273.

[25] T. Tayebi, A. J. Chamkha, A. A. Melaibari, and E. Raouache, Effect of internal heat generation or absorption on conjugate thermal-free convection of a suspension of hybrid nanofluid in a partitioned circular annulus, International Communications in Heat and Mass Transfer. 126 (2021) 105397.

[26] T. Tayebi and A. J. Chamkha, Natural convection enhancement in an eccentric horizontal cylindrical annulus using hybrid nanofluids, Numerical Heat Transfer, Part A: Applications. 71 (2017) 1159–1173.

[27] A. A. Charab, S. Movahedirad, and R. Norouzbeigi, Thermal conductivity of Al 2 O 3 + TiO 2 /water nanofluid: Model development and experimental validation, Applied Thermal Engineering. 119 (2017) 42–51.

[28] H. C. Brinkman, The Viscosity of Concentrated Suspensions and Solutions, The Journal of Chemical Physics. 20 (1952) 571–571.

[29] C. H. Cho, K. S. Chang, and K. H. Park, Numerical Simulation of Natural Convection in Concentric and Eccentric Horizontal Cylindrical Annuli, Journal of Heat Transfer. 104 (1982) 624–630.

[30] L. S. Yao and F. F. Chen, Effects of Natural Convection in the Melted Region Around a Heated Horizontal Cylinder, Journal of Heat Transfer. 102 (1980) 667–672.